

Modeling of turbulent MHD processes on the Sun

By I. N. Kitiashvili, A. G. Kosovichev[†], N. N. Mansour[‡] AND A. A. Wray[‡]

Solar observations from the ground and in space show a complicated interaction of highly turbulent plasma ($Re \sim 10^{12}$) and magnetic fields. The turbulent MHD processes result in the concentration of magnetic fields into compact structures, observed as sunspots, pores, or small bright magnetic regions. These observations lead to high-speed (~ 450 km/s) ejection of magnetized plasma (coronal mass ejection), high-temperature solar flares, and other phenomena. Numerical modeling of MHD phenomena in the solar plasma provides us with better understanding of the nature of the turbulent structures and their dynamics. In this paper, we discuss the dynamics of solar turbulent convection in different conditions: from quiet Sun conditions (with zero or weak magnetic field) to sunspot conditions (with strong magnetic fields of ~ 1 kG and greater), obtained from analysis of the radiative MHD LES simulations carried out at the CTR. In particular, we discuss the role of turbulent vortices in the mechanism of spontaneous formation of magnetic structures and the driving mechanism of high-speed flows in the filamentary structure of sunspots.

1. Introduction

Realistic numerical simulations of fluid dynamics and magnetism in the Sun are very important for the analysis and interpretation of observational data from ground-based observations and space missions, such as the Solar and Heliospheric Observatory (ESA/NASA), Solar-B/Hinode (Japan/NASA), and Solar Dynamics Observatory (NASA). Also, simulations become increasingly important for developing physics-based methods of space-weather forecasts that are essential for future space exploration, both manned and unmanned. Realistic numerical simulations pioneered by Stein & Nordlund (2001) have provided important insights into the structure and dynamics of solar convection and the excitation mechanisms of oscillations in the Sun and in solar-type stars. These simulations represent properties of acoustic waves generated by turbulent motions and nonadiabatic pressure fluctuations (Jacoutot *et al.* 2008a,b).

The CTR – NASA Ames group has developed a highly efficient parallel radiative magnetohydrodynamics code for 3D simulations of solar turbulent convection in magnetic field regions. The code includes all essential physics from first principles and includes various subgrid-scale LES turbulence models. The implementation of this code on the NASA/Ames supercomputer systems Columbia and Pleiades shows a very efficient, nearly 100% scaling for a large number of processors. The code has been applied for realistic simulations of solar convection in different magnetic field strengths and inclinations. The results reveal very interesting dynamics and show self-organization processes of solar magnetoconvection, reproduce several phenomena observed in solar active regions, provide an explanation for the high-speed shear flows (Evershed effect) in sunspots, and demonstrate possible mechanisms for the formation of stable magnetic structures.

[†] HEPL, Stanford University, USA

[‡] NASA Ames Research Center, USA

2. Basic equations and numerical setup

The realistic simulations of solar convection and oscillation in the presence of magnetic fields reveal very interesting dynamics, reproducing several phenomena observed in solar active regions. The 3D radiative MHD simulation code ("SolarBox", developed by A. Wray) is based on a LES formulation and includes various subgrid-scale turbulence models. The code has been carefully tested and used for studying how various turbulence models affect the excitation of solar acoustic oscillations by turbulent convection in the upper convection zone (Jacoutot *et al.* 2008a,b). This code takes into account several physical phenomena: compressible fluid flow in a highly stratified medium; three-dimensional multi-group radiative energy transfer between the fluid elements; a real-gas equation of state; ionization and excitation of all abundant species; and magnetic effects. Because both the Reynolds number and magnetic Reynolds number are very high, an important feature of this code is implementation of various subgrid-scale LES turbulence models. Here we adopted the most widely used Smagorinsky model (Smagorinsky 1963) and its compressible dynamic formulation (Moin *et al.* 1991; Germano *et al.* 1991). The turbulent electrical conductivity is calculated by using an extension of the Smagorinsky model for the MHD case (Theobald *et al.* 1994). Also, during the CTR Summer Program subgrid-scale models developed by Balarac *et al.* (2010) have been implemented and used in the simulations.

The governing equations are the grid-cell averaged equations for the conservation of mass (2.1), momentum (2.2), energy (2.3), and magnetic flux (2.4):

$$\frac{\partial \rho}{\partial t} + (\rho u_i)_{,i} = 0, \quad (2.1)$$

$$\frac{\partial \rho u_i}{\partial t} + (\rho u_i u_j + (P_{ij} + \rho \tau_{ij}))_{,j} = -\rho \phi_{,i}, \quad (2.2)$$

$$\frac{\partial E}{\partial t} + \left[E u_i + (P_{ij} + \rho \tau_{ij}) u_j - (\kappa + \kappa_T) T_{,i} + \left(\frac{c}{4\pi} \right)^2 \frac{1}{\sigma + \sigma_T} (B_{i,j} - B_{j,i}) B_j + F_i^{rad} \right]_{,i} = 0, \quad (2.3)$$

$$\frac{\partial B_i}{\partial t} + \left[u_j B_i - u_i B_j - \frac{c^2}{4\pi(\sigma + \sigma_T)} (B_{i,j} - B_{j,i}) \right]_{,j} = 0, \quad (2.4)$$

where ρ is the average mass density, u_i is the Favre-averaged velocity, B_i is the magnetic field, and E is the average total energy density $E = \frac{1}{2} \rho u_i u_i + \rho e + \rho \phi + \frac{1}{8\pi} B_i B_i$, where ϕ is the gravitational potential and e is the Favre-averaged internal energy density per unit mass. F_i^{rad} is the radiative flux, which is calculated by solving the radiative transfer equation, and P_{ij} is the averaged stress tensor $P_{ij} = (p + \frac{2}{3} \mu u_{k,k} + \frac{1}{8\pi} B_k B_k) \delta_{ij} - \mu (u_{i,j} + u_{j,i}) - \frac{1}{4\pi} B_i B_j$, where μ is the viscosity. The gas pressure p is a function of e and ρ calculated through a tabulated equation of state (Rogers *et al.* 1996); τ_{ij} is the Reynolds stress, κ is the molecular thermal conductivity, κ_T is the turbulent thermal conductivity, σ is the molecular electrical conductivity, and σ_T is the turbulent electrical conductivity.

The simulation results are obtained for the computational domain of $6.4 \times 6.4 \times 5.5$ Mm with various grid sizes: $50 \times 50 \times 43$ km, $25 \times 25 \times 21.7$ km and $12.5 \times 12.5 \times 11$ km. The domain includes a 5 Mm-deep layer of the upper convective zone and the low atmosphere. The lateral boundary conditions are periodic. The top and bottom boundaries are closed to mass, momentum and energy transfer (apart from radiative losses), and maintain the total magnetic flux and the mean inclination in the simulation domain. Also, there is no

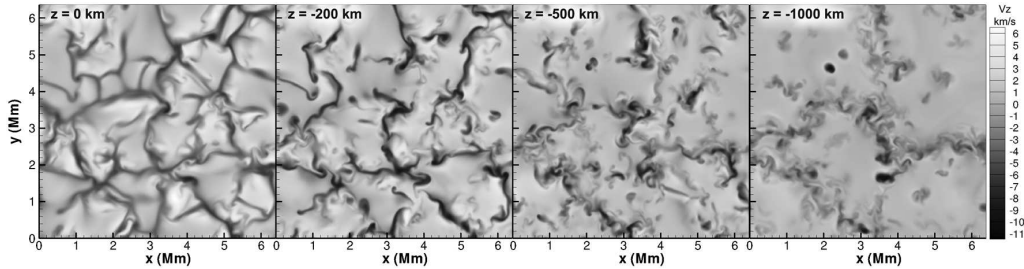


FIGURE 1. Snapshots of the vertical velocity at different depths z from the surface to 2000 km below the solar surface (from right to left).

net magnetic field lost or gained through the boundaries, i.e., integral over volume for each component of the field is constant. The results have been verified by increasing the computational domain size to 12.8 Mm in the horizontal directions. The initial uniform magnetic field is imposed on a snapshot of the preexisting hydrodynamic convection. The initial field strength, B_0 , varies from 0 to 2000 Gauss, and the inclination angle, α , varies from vertical (0°) to horizontal (90°). This formulation allowed us to carry out a series of controlled numerical experiments and investigate how the structure and dynamics of solar turbulent convection depends on the magnetic field properties. In section 3 we discuss the turbulent convection properties in the simulations without of magnetic field (“quiet Sun” model). In section 4 we present results of simulations of processes of magnetic self-organization, filamentary structurization and high-speed shear flows in the turbulent magnetized plasma.

3. Simulations of the quiet Sun

Numerical simulations of the properties of convection in quiet-Sun regions (where the magnetic field is weak or absent) are important for investigating the dynamics of solar convective structures such as granulation and supergranulation that form under highly turbulent conditions. One interesting property is the multiscale character of convective motions at different depths. However, the question of scale separation, which is important for dynamo theories (see Yokoi *et al.* 2010) and for theories of magnetic structurization (see Rogachevskii *et al.* 2010), is still open[†]. Simulation of the solar surface demonstrates a “boiling” behavior of convective cells (granules) with size 1000 – 2000 km, very similar to observations. Deeper down we see in the simulation results the formation of larger-scale structures. Figure 1 shows snapshots of the vertical velocity at different depths, from the surface to 2000 km-deep layers. Dark areas correspond to downflows that sometimes reach supersonic speed, up to 11 km/s (Mach number ~ 1.5). Figures 2a, b shows snapshots for temperature (left column) and density (right) at the surface for a case with no magnetic field. The convective motions at the simulated solar surface represent granulation patterns with the hotter and less dense upflowing plasma in the middle of the granular cells, and the lower temperature and higher density in downflowing plasma at the intergranulation boundaries (dark lines of granulation).

The existence of horizontal supersonic flows in the granular convection initially was predicted by numerical simulations (Stein & Nordlund 1998) and recently found in observations by the Solar Optical Telescope on the Hinode spacecraft (Bellot Rubio 2009).

[†] Recent analysis of laboratory experiments of convection shows the possibility of separation of different scales (Bukai *et al.* 2009).

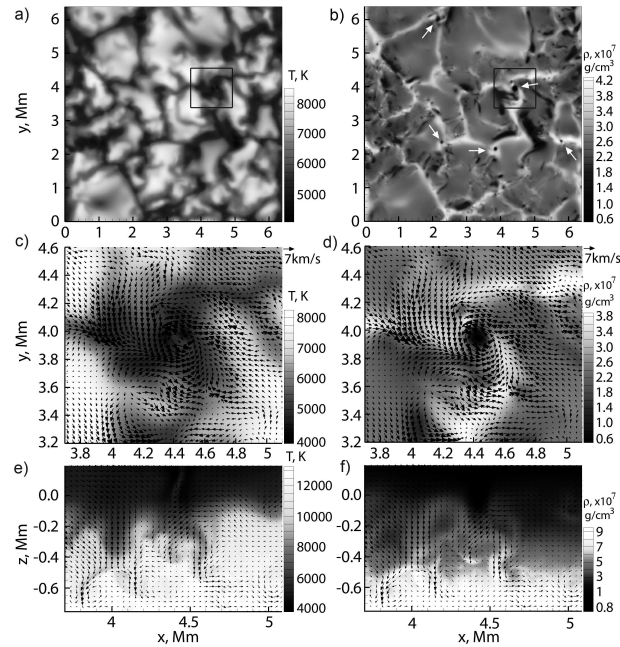


FIGURE 2. Snapshots of granular convection at the surface for a simulation without magnetic field, with a horizontal resolution of 12.5 km: temperature (left column) and density (right). The black square indicates a large vortex tube (whirlpool), the horizontal and vertical structure of which are shown separately in panels c) – f). Black arrows show the flow velocity. White arrows in panel b) point to the centers of some vortices (dark low-density points).

Our simulation results reveal a direct connection between the supersonic horizontal flows and vortex tubes, whirlpool-like motions, that have various sizes ($\sim 0.2 - 1$ Mm) and lifetimes ($\sim 15 - 20$ min) and are typically formed at the vertices of the intergranular lanes.

The vortical motions are seen particularly well in the density variations. The centers of the whirlpools are seen as dark dots (indicated by white arrows in Figure 2b) in the intergranular space. The evolution of these vortices is ultimately related to the dynamics of convective motions. The convective flows may sometime collect swirls in a local area, then merge and destroy them. Such vortical structures in simulations were first described by Stein & Nordlund (1998). They showed that stronger vortices usually correlate with downflows, and this correlation is also found in our results.

From time to time, convection creates big whirlpools, such as the one indicated by the square in Figure 2. These big whirlpools can swallow up other smaller swirls around them. The big swirls are usually easy to see not only in the density but also in the surface temperature and intensity variations. The detailed structure of a large whirlpool is shown in Figures 2c, d. The whirlpool structure is characterized by: i) formation of downdraft lanes (visible as "arms" in the Figures 2c, d) of higher density that correlates with lower temperature; ii) a pronounced vortical structure of the velocity field; iii) increased magnitude of the horizontal velocity up to 7 – 11 km/s; iv) a sharply decreased density in the central core of the vortex, and a slightly higher temperature than in the surrounding area. The typical depth of large swirls is about 100 – 200 km. Inside the whirlpool (Figure 2e) we can see a higher-temperature sheet-like structure, but it

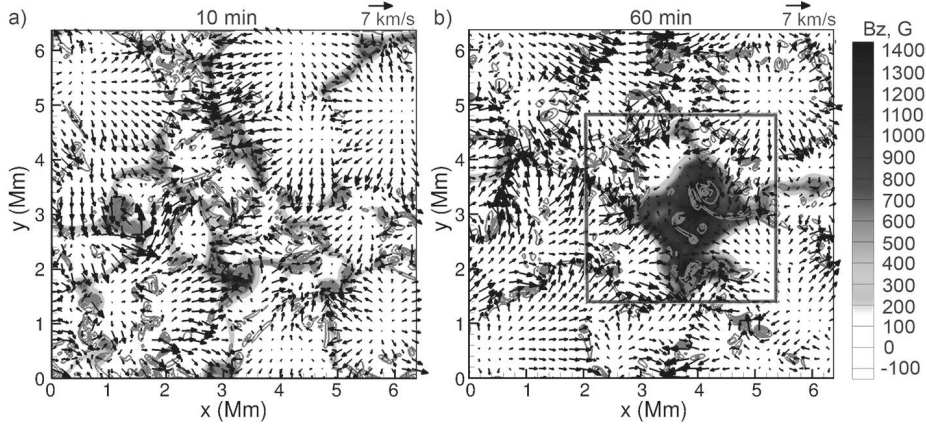


FIGURE 3. Snapshots of the surface distribution of vertical magnetic field (background), horizontal flows (arrows,) and vorticity magnitude (gray contour lines) for four moments of time: 10 and 60 min, from the moment of initiation of a uniform magnetic field ($B_{z0} = 100$ G).

is unstable (in comparison with the whirlpool lifetime), and can be destroyed during the swirling motions. Vortical motions in solar granulation have been detected in high-resolution observations (e.g. Bonet *et al.* 2008), and the observational results generally agree with the simulations. In addition, recent observations of a quiet region, near the solar disk center, detected magnetic bright points following a logarithmic spiral trajectory around intergranular points and then engulfed by a downdraft (Bonet *et al.* 2008).

4. Self-organization processes in turbulent magnetoconvection

4.1. Convection in a vertical magnetic field

To investigate the process of magnetic field structuring in a turbulent convective plasma, we made a series of simulations for an initial vertical uniform magnetic field, B_{z0} , varying from 1 to 100 G, using various computational grids and domain sizes. Qualitatively the simulation results are very similar in all the cases, and show formation of compact stable magnetic pore-like structures. In Figure 3 we present results for the case of $B_{z0} = 100$ G, a grid size of 25 km, and a domain size of $6.4^2 \times 5.5$ Mm, for which we have made the longest run (9 hours of solar time). The periodic lateral boundary conditions allow us, for the purpose of illustration, to shift the horizontal frame so that the structure is located close to the center. As we see in the simulations, the structure can be formed any place in our computational domain, but usually the process starts at one of the strongest vortices (Kitiashvili *et al.* 2010).

Figure 3 shows two snapshots of the vertical magnetic field (background image), horizontal flow field (arrows), and vorticity magnitude (contour lines) for four moments of time: 10 and 60 min after the moment $t = 0$, when the 100 G vertical field was uniformly distributed into the computational domain. During the first few minutes the magnetic field is swept into the intergranular lanes and is significantly amplified up to $\sim 500 - 1000$ G. The vortices and magnetic field concentrate at some locations in the intergranular lanes, where they are deformed and become elongated (or elliptically shaped) along the intergranular lines. The process of formation of a large-scale magnetic structure starts at the strongest vortex in our domain. This large swirl drags magnetic field and also becomes stretched by strong horizontal shear flows. The whirlwind causes deforma-

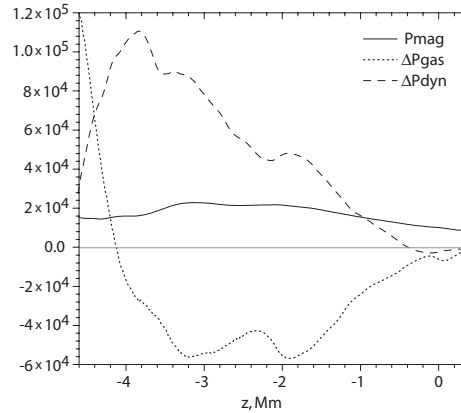


FIGURE 4. Total magnetic pressure (solid black curve) averaged over a rectangular area, which contains the magnetic structure (indicated in Figure 3), and the differences of the gas (dotted curve) and dynamic pressure (dashed curve), calculated in the magnetic structure area and in the surrounding region. The variations in the magnetic, gas, and dynamic pressure are averaged over 10 min.

tion of the intergranular space, and creates a cavity of low density, temperature, and pressure. The cavity expands and increases the accumulation of magnetic field. A similar process of magnetic field concentration, sweeping, twisting, and stretching by vortical motions in the intergranular lane was initially observed in the simulations of Stein *et al.* (2003). However, the previous simulations did not show formation of a large-scale structure, presumably due to different resolution and depth of the domain.

During the next few minutes the deformation of the "parent" vortex continues; then it is destroyed on the surface by $t = 10$ min (Figure 3a), but leaves strong downdraft motions in the interior. The process of accumulation of magnetic flux in this area continues. The local concentrations of magnetic field and vorticity get stronger and are moved by convective motions in the direction of the initial cavity, into the region where the gas pressure remains systematically low due to the downdrafts. In Figure 3a several small-scale structures can be seen in this area. However, it is difficult to recognize the future center of the attraction on the surface. Collisions of flows coming from different directions create additional vortices, and this seems to accelerate the accumulation process. As a result, the different small magnetic structures join together in a magnetic conglomerate that continues to attract other magnetic micro-structures and becomes more compact (Figure 3b). By $t = 60$ min, the magnetic field is mostly concentrated in a single flux tube-like structure with a maximum field strength of about ~ 4 kG at a depth of $\sim 1 - 4$ Mm, and $\sim 1.4 - 1.5$ kG at the surface. The magnetic field is weaker and more disperse near the bottom of our domain, which is impenetrable. The flux-tube interior represents a cluster-type structure, initially predicted by Parker (1979) and observed on a larger scale for a sunspot by helioseismology (Zhao *et al.* 2010). In our simulations the cluster-type structure is represented by internal field concentrations (flux tubes), 100 – 200 km thick, in which the field strength reaches 6 kG after 1 hour (Kitiashvili *et al.* 2010). The velocity distribution shows strong, often supersonic, downflows around the magnetic structure. Inside the magnetic structure the convective flows are suppressed by the strong magnetic field. However, despite the weak velocities ($\sim 0.1 - 0.2$ km/s) there are very small elongated convective cells resembling umbral dots observed at the surface. The distribution of density fluctuations shows the following basic properties: i) decrease of

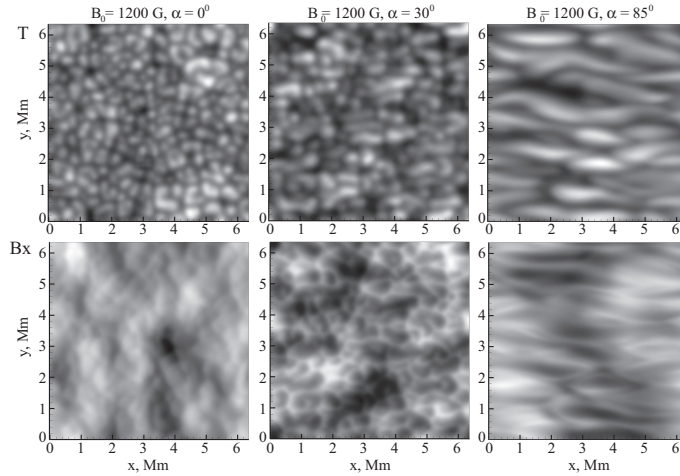


FIGURE 5. Evolution of intensity ($\lambda = 4504.4\text{\AA}$, top row) and horizontal magnetic field (bottom row) for magnetoconvection in the presence of an inclined magnetic field of 1200 G with inclination angles from the vertical of: 0° , 30° , and 85° .

density inside the magnetic structure; ii) fine needle-like structurization; iii) a thin near-surface layer of slightly higher density; and iv) higher density around the structure, particularly in the deep layers of the domain. We have followed the evolution of the magnetic pore-like structure for more than 9 solar hours, and did not see any indication of its decay. However, the shape and other properties fluctuate during this evolution (Kitiashvili *et al.* 2010). Decay of this structure may be prevented by keeping the total magnetic flux constant in the domain during the run. We repeated the simulation when the initial uniform magnetic field was introduced at a different moment of time. In one case we observed the formation of two separate magnetic structures, which later merged together, but the whole process was very similar. Weak-magnetic field simulations (1 – 10 G) also demonstrate the accumulation of magnetic field. However, the area of the magnetic field concentration is much smaller and located in a narrow intergranular lane.

The precise role of various factors contributing to structure formation is not yet established. In Figure 4, we plot, as a function of depth, the magnetic pressure averaged over a rectangular area (indicated in Figure 3), which contains the magnetic structure. Also, we plot the differences between the gas and dynamic pressure, calculated in this area and in the surrounding region. In the upper 0.5 Mm, both the gas and dynamic pressure are suppressed. In the deeper interior, the gas pressure is sharply reduced, but the dynamic pressure is increased, and these changes significantly exceed the magnetic pressure. This indicates that magnetic structure formation is not caused by a thermal collapse effect due to radiative cooling at the surface but is probably due to a significant suppression of the gas pressure in the deep layers. This suppression is accompanied by an increase of the total dynamic pressure (calculated as $\frac{1}{2}\rho|\vec{u}|^2$). We emphasize that this discussion is preliminary. These processes are currently being investigated in detail.

4.2. Filamentary structure formation in an inclined magnetic field

The magnetoconvection picture becomes even more interesting for the case of an inclined field, because the magnetic field inclination dramatically changes the shape of convective cells. Figure 5 shows an example of the shape changes for the temperature (top row) and horizontal magnetic field (bottom) distributions at the surface, in the magnetoconvection

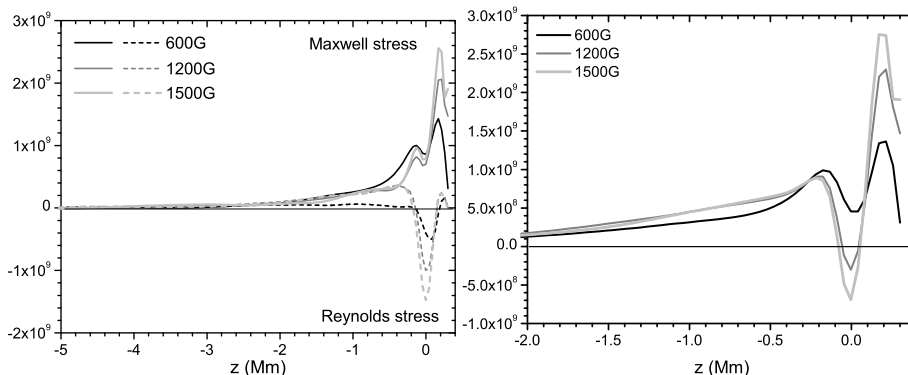


FIGURE 6. Variations of the Maxwell and Reynolds stresses (left panel), and their sum (right panel) obtained from the simulation results for initial magnetic field strengths of 600, 1200, and 1500 G, inclined at 85° from the vertical.

simulations for initial magnetic field $B_0 = 1200\text{G}$ and different magnetic field inclination angles from the vertical of: 0° , 30° , and 85° . In the case of a vertical initial magnetic field ($\alpha = 0^\circ$), we see the usual small granules more or less uniformly distributed. For a weakly inclined field ($\alpha = 30^\circ$) the convective granules have an elongated structure. The horizontal component of magnetic field then has a web-like structure of local field concentrations. In the case of an almost horizontal magnetic field ($\alpha = 85^\circ$), the magnetoconvection shows a highly filamentary structure in both the temperature and magnetic field distributions.

In the highly inclined magnetic field case the whole convective pattern is moving in the direction of inclination in a manner similar to running convective waves (Kitiashvili *et al.* 2009). The flow speed is accelerated up to 6 km/s for $\alpha = 85^\circ$. Increasing the initial magnetic field strength speeds up the horizontal flows and makes the elongated convective cells narrower. These properties are dramatically different from solar convection without magnetic field or in the presence of a vertical magnetic field, where the convection forms granulation cells, the size of which decreases with increasing magnetic field strength (e.g., Jacoutot *et al.* 2008b).

The filamentary structure of magneto-convection corresponds to the penumbrae of sunspots. The high-speed flow patches are observed in high-resolution observations of sunspots, and are called "Evershed clouds". This flow is highly non-stationary, reflecting the nature of the overturning magnetoconvection. The characteristic time of these flows is 5 – 20 min. This flow is known in solar physics as the "Evershed effect" (Evershed 1909). The simulations show that the maximum speed of the mean shear flow increases with depth in the visible layers of the Sun, which also corresponds to the observations.

It is interesting that the simulation results (Kitiashvili *et al.* 2009) provide a synergy of the early proposed models: propagation of the flows in weakly-magnetized gaps in the magnetic field (Severnyi 1965), the thin-flux tube model (Schlichenmaier *et al.* 1998), the siphon model (Meyer & Schmidt 1968), the overturning convection model (Scharmer *et al.* 2008), and the convective rolls model (Busse 1987). In particular, our analysis shows that the oscillatory behavior of the convective rolls has some agreement with the simulation results. As indicated by the convective rolls theory, the balance between the Reynolds and Maxwell stresses (Figure 6) in subsurface layers can be a driving force of the Evershed effect.

5. Conclusion

Radiative MHD simulations of the subsurface turbulent layer of the Sun have greatly improved our understanding of the multi-scale structure and dynamics of solar convection. A characteristic feature of simulations of this type is that they include all essential physics from first principles, but they do rely on subgrid-scale models of turbulence. In this paper, we have presented different regimes of the turbulent convection from a purely hydrodynamic case to a highly magnetized plasma. During the CTR Summer Program it was found that the effects of turbulence including subgrid-scale effects (see also Rogachevskii *et. al* (2010)) play a critical role in the mechanism of magnetic structure formation in the solar plasma. In this mechanism, the initial local instability is created by vortex tubes with strong downflows, which initiate the concentration of the vertical magnetic field into magnetic flux tubes. The increased subsurface downflows create a region of reduced gas pressure, which becomes a region where the flux tubes are collected into a single large-scale structure.

The physical picture of turbulent magnetoconvection in almost horizontal strong magnetic field regions, representing sunspot penumbra, is the following. Convective cells are deformed under the action of the inclined magnetic field, forming filamentary structures and producing high-speed Evershed flows (Kitiashvili *et al.* 2009). The magnetic field lines are stretched by the downward flows and dragged under the surface. The points where the magnetic field lines cross the solar surface are observed as magnetic patches of positive and negative polarities (the so-called sea-serpent structure).

The next challenge for the simulations is to provide a full self-organized model of sunspots, including both the central umbra with a predominantly vertical magnetic field, surrounded by a penumbra with an almost horizontal field.

Acknowledgments. This work was supported by the Center for Turbulence Research (Stanford) and NASA Ames Research Center.

REFERENCES

- BALARAC, G., KOSOVICHEV, A., BRUGIÈRE, O., WRAY, A. & MANSOUR, N. 2010 Modeling of the subgrid-scale term of the filtered magnetic field transport equation. *Proc. of CTR Summer Program*.
- BELLOT RUBIO, L. R. 2009 Detection of supersonic horizontal flows in the solar granulation. *ApJ* **700**, 284–291.
- BONET, J. A., MÁRQUEZ, I., SÁNCHEZ ALMEIDA, J., CABELLO, I. & DOMINGO, V. 2008 Convectively driven vortex flows in the Sun. *ApJ* **687**, L131–134.
- BUKAI M., EIDELMAN A., ELPERIN T., KLEEORIN N., ROGACHEVSKII I. & SAPIRKATIRAIE I. 2008 Effect of large-scale coherent structures on turbulent convection. *Physical Review E* **79**, 066302 (1–9).
- BUSSE, F. H. 1987 A new mechanism for the Evershed flow. In *Proc. of the Inaugural workshop*, 187–196.
- EVERSHED, J. 1909 Radial movement in sun-spots. *MNRAS* **69**, 454–457.
- GERMANO, M., PIOMELLI, U., MOIN, P., & CABOT, W. H. 1991 A dynamic subgrid-scale eddy viscosity model. *Physics of Fluids* **3**, 1760–1765.
- JACOUTOT, L., KOSOVICHEV, A. G., WRAY, A., & MANSOUR, N. N. 2008a Realistic

- numerical simulations of solar convection and oscillations in magnetic regions. *ApJ* **684**, L51–L54.
- JACOUTOT, L., KOSOVICHEV, A. G., WRAY, A., & MANSOUR, N. N. 2008b Numerical simulation of excitation of solar oscillation modes for different turbulent models. *ApJ* **682**, 1386–1391.
- KITIASHVILI I. N., KOSOVICHEV A. G., WRAY A. A. & MANSOUR N. N. 2009 Traveling waves of magnetoconvection and the origin of the Evershed effect in sunspots. *ApJ* **700**, L178–L181.
- KITIASHVILI I. N., KOSOVICHEV A. G., WRAY A. A. & MANSOUR N. N. 2010 Mechanism of spontaneous formation of stable magnetic structures on the Sun. *ApJ* **719**, 307–312.
- MEYER, F. & SCHMIDT, H. U 1968 The Evershed effect as a wave phenomenon. *Mitteilungen der Astronomischen Gesellschaft Hamburg* **25**, 194–196.
- MOIN, P., SQUIRES, K., CABOT, W. & LEE, S. 1991 A dynamic subgrid-scale model for compressible turbulence and scalar transport. *Phys. Fluids A* **3**, 2746–2757.
- PARKER, E. N. 1979 Sunspots and the physics of magnetic flux tubes. I - The general nature of the sunspot. II - Aerodynamic drag. *ApJ* **230**, 905–923.
- ROGACHEVSKII, I., KLEEORIN N., KITIASHVILI I. N., KOSOVICHEV A. G., WRAY A. A., & MANSOUR N. N. 2010 LES of turbulent convection in solar-type stars and formation of large-scale magnetic structures. *Proc. of CTR Summer Program*.
- ROGERS, F. J., SWENSON, F. J & IGLESIAS, C. A. 1996 OPAL Equation-of-State tables for astrophysical applications. *ApJ* **456**, 902–908.
- SCHLICHENMAIER, R., JAHN, K. & SCHMIDT, H. U. 1998 A dynamical model for the penumbral fine structure and the Evershed effect in sunspots. *ApJ* **493**, L121–L124.
- SCHARMER, G. B., NORDLUND, Å., & HEINEMANN, T. 2003 Solar surface magnetoconvection. *ApJ* **677**, L149–L152.
- SEVERNYI, A. B. 1965 The nature of solar magnetic fields (the fine structure of the field). *Soviet Astronomy* **9**(1), 171–182.
- SMAGORINSKY, J. 1963 General circulation experiments with the primitive equations I. The basic experiment. *Monthly Weather Review* **93**(1), 99–164.
- STEIN, R. F., & NORDLUND, Å 1998 Simulations of solar granulation. I. General properties. *ApJ* **499**, 914–933.
- STEIN, R. F., & NORDLUND, Å 2001 Solar oscillations and convection. II. Excitation of Radial Oscillations. *ApJ* **546**, 585–603.
- STEIN, R. F., BERCIK, D. & NORDLUND, Å. 2003 Solar surface magneto-convection. *ASP Conf. Series* **286**, 121–131.
- THEOBALD, M. L., FOX, P. A., & SOFIA, S. 1994 A subgrid-scale resistivity for magnetohydrodynamics. *Phys. Plasmas* **1**(9), 3016–3032.
- YOKOI, N., BALARAC, G., KITIASHVILI, I. N., KLEEORIN, N., KOSOVICHEV, A. G., ROGACHEVSKII, I. & SIMITEV, R. 2010 Integrated exploration of turbulent cross-helicity effect: theory, observation, modeling and numerical simulations of the solar convection zone. *Proc. of CTR Summer Program*.
- ZHAO, J., KOSOVICHEV, A. G. & SEKII, T. 2010 High-resolution helioseismic imaging of subsurface structures and flows of a solar active region observed by Hinode. *ApJ* **708**, 304–313.